XMM-Newton

XMM-Newton Science Analysis System (version 6.5)
EPIC Science Validation Report

XMM-SOC-USR-TN-0009 Issue 2.0

M. Guainazzi, C.Gabriel, B.Altieri, I.Caballero, M.Ehle, J.Hoar,
M.G.F.Kirsch, A.Pollock, R.Saxton, M.Stühlinger, A.Talavera
XMM-Newton Science Operations Center

J.Osborne, C.Page, I.Stewart, M.Watson
XMM-Newton Science Survey Center

16 August 2005

Revision history

Revision number	Date	Revision author	Comments
0.1	29 January 2004	M.Guainazzi	LATEX template
0.2	5 March 2004	M.Guainazzi	First complete draft
0.3	15 March 2004	M.Guainazzi	Second complete draft (after SOC/SSC-LUX comments)
0.4	23 March 2004	M.Guainazzi	Third complete draft (after SOC/SSC comments)
1.0	24 March 2004	M.Guainazzi	Public version for SASv6.0
2.0	16 August 2005	M.Guainazzi	Public version for SASv6.5 (only EPIC part of the validation addressed)

Contents

1 Introduction

1.1 Concept

Scientific Validation (SV) is required in order to ensure a constant high quality of the XMM-Newton Science Analysis System (SAS).
The main purpose of the SV is to provide the SAS community with a stable reliable software product, as well as to generate a list of caveats and known deficiencies. Together with these "functional" tests, the SV provides some information on the expected systematic uncertainties when basic data analysis products are generated through the current version of the SAS, using the best calibrations available at the moment SAS was released. It is important to stress that *this document does not supersede or substitute* the **instrument calibration status documents**, available from the XMM-Newton calibration portal. Instrument calibration is a continuous activity, whose results (update of calibration files) is intrinsically and necessarily decoupled from software releases. XMM-Newton users are recommended to consult periodically the URL: `http://xmm.vilspa.esa.es/calibrations`, which informs on the calibration status of the XMM-Newton instruments.
The document you are reading (*SAS Science Validation Report*) contains information about:

- which instrumental modes are fully supported by SAS,
- which scientific products SAS can produce,
- the level of accuracy associated with those products,
- a list of caveats and problems.

The SV is performed on a standard set of XMM-Newton observations, which cover all commissioned observational modes. Tab. 1 lists all the datasets used for the validation of SAS version 6.5 (*SAS v6.5* hereinafter). Some of these observations are particularly suitable to test calibration-related items, as specified in the rightmost column of Tab. 1. These datasets are intended as a standard reference, which has been and will be used to verify the performances of all SAS versions. However, additional datasets may occasionally be used to test version-specific SAS items. This is the case, for instance, for the datasets discussed in Sect. 2.2 of this report. Datasets discussed in a given report and not listed in Tab. 1 do not belong to the reference datasets, and are therefore not intended to be discussed in later SAS versions validation reports.

1.2 Methodology

The SV for SAS v6.5 consisted of the following steps:

1. the same datasets are also processed through the SAS reduction meta-tasks: `e[mp]proc`, `e[mp]chain`, `om[ifg]chain`, `rgsproc`
2. products generated by the above step were used as basis for the *interactive SV analysis*. Standard scientific products (images, light curves, spectra, source lists) are generated and analyzed. This allows to:
   - test the SAS interactive tasks.
   - verify the calibration accuracy obtained with SAS v6.5, and compare it with the expected accuracy on the basis of the calibration status at the time the SV is performed.

Table 1: SV datasets

Instrument	Mode	Object	Revolution Observation ID	Dataset ID	Calibration item
EPIC MOS	Full Frame	Lockman Hole	070 0123700101	1	Astrometry
	”	G21.5.09	060 0122700101	2	Effective area
	Small Window (W2)	Mkn 421	165 0099280201	3	
	Large Window (W3)	PKS0558-504	153 0129360201	4	Effective area
	Timing Uncompressed	Her X-1	207 0134120101	5	Timing
EPIC-pn	Full Frame	Lockman Hole	070 0123700101	1	Astrometry
	Full Frame/Small Window	PKS0558-504	153 0129360201	4	Effective area
	Large Window	AB Dor	185 0133120201	6	
	Small Window	PKS0558-504	084 0125110101	7	Effective area
	Fast Timing	Her X-1	207 0134120101	5	Timing
		Crab	411 0153750401	8	
	Fast Burst	Crab	411 0153750301	9	Timing
		Crab	411 0153750501	10	Timing
	Extended Full Frame	G21.5-0.9	060 0122700101	2	Effective area
RGS	SPEC+Q	PKS0558-504	084 0125110101	7	
”		Mkn 421	165 0099280201	3	Effective area
	”	AB Dor	185 0133120201	6	Wavelength scale
	”	AB Dor	338 0134521301	11	Wavelength scale
	”	AB Dor	462 0134521601	12	Wavelength scale
	”	AB Dor	572 0134522201	13	Wavelength scale
OM	Image Mode	BPM 16274	261 0125320701	14	Photometry
	Fast Mode	X1822-371	228 0111230101	15	
	FF Low Resolution	BPM 16274	261 0125320701	14	Astrometry
	Optical grism	Hz2	503 0125910901	16	Wavelength scale & flux calibration
	UV Grism	HD13499 (offset)	657 0125911301	17	Wavelength scale & flux calibration

Table 2: Best-fit parameters and results when a photoelectrically absorbed power-law model is applied to the EPIC spectra of G21.5-0.9

Camera	N_H (10^{22} cm^{-2})	Γ	2-10 keV flux (10^{-11} cgs)
MOS1	2.16 ± 0.04	1.85 ± 0.03	6.13 ± 0.05
MOS2	2.16 ± 0.04	1.90 ± 0.03	5.91 ± 0.05
pn	2.13 ± 0.03	1.856 ± 0.016	6.16 ± 0.03

The conclusions of the SV are summarized in Sect. 5. A list of instrument modes supported by SAS v6.5 is reported in Appendix A. A summary of SAS v6.5 capabilities is detailed in Appendix B.
In this report: best-fit parameter uncertainties are at the 90% confidence level for 1 interesting parameter ($\Delta\chi^2 = 2.71$); errors on positions or count rates are at the 1-σ level; energies are quoted in the observer's reference frame unless otherwise specified.
Issue 2.0 of this document contains the results of the SASv6.5 SV for the EPIC cameras only. A full document, including the SV results for RGS and OM as well, will be published later.

2 EPIC camera imaging modes

2.1 EPIC cameras effective area

2.1.1 G21.5-0.9

The X-ray spectrum of the Crab-like SuperNova Remnant (SNR) G21.5-0.9 (Warwick et al. 2001) is well described by a strongly absorbed (column density, $N_H \sim 2 \times 10^{22}$ cm^{-2}) power-law. At 0-th order, it can be characterized through 3 quantities only: N_H, the photon index Γ and the model normalization or flux. This source is therefore particularly well-suited to compare the performances of the response matrices above 1 keV.
The XMM-Newton observation discussed in this report was performed on April 7, 2000. The EPIC cameras were operating in Full Frame (MOS), and Extended Full Frame (pn) mode, respectively. The source was on-axis. Data were reduced with both the `chains` and the `procs` EPIC reduction meta-tasks. Although the resulting event lists are not completely identical due to residual small infrastructure differences, we have verified that the spectral results described hereafter are indistinguishable at the last significant digits.
Source spectra were extracted from circular regions of $2.7'$ radius around the centroid of the SNR. Background spectra were extracted from annuli of $3.15'$ to $4.6'$ radius. The source spectra were rebinned in order to have at least 50 counts in each spectral bin and to oversample the instrumental energy resolution by a factor not higher than 3. The spectra were fit in the 0.5-10 keV and 0.3-10 keV energy bands for MOS and p-n, respectively. Effective areas were generated using exposure-specific detector maps, as recommended for extended sources. As already stressed in the SASv6.0 Science Validation Report, wrong results are obtained, if one uses a *flat* detector map in either `arfgen` or `rmfgen`.
The best-fit results are shown in Tab. 2 and Fig. 1, and Fig. 2. Residuals are within $\pm 5\%$ across the whole sensitive bandpass of the EPIC cameras. The MOS 2 cameras exhibits a steeper spectrum ($\Delta\Gamma \lesssim 0.05$), and a lower 2–10 keV flux by $\simeq 4\%$. Otherwise, the best-fit parameters

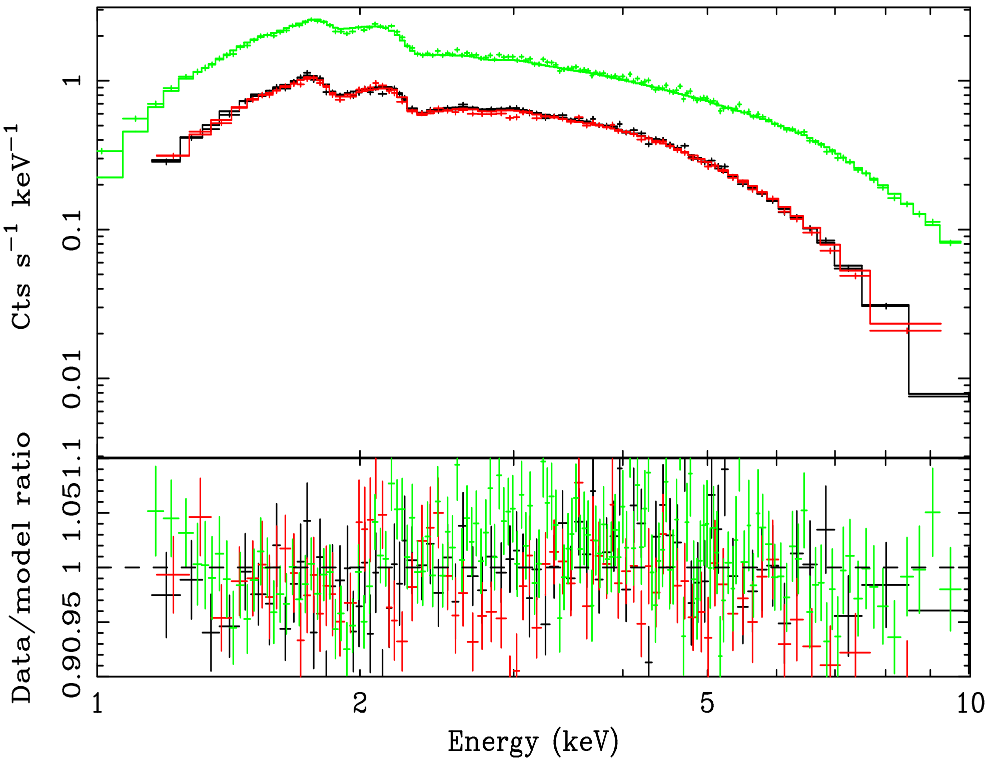

Figure 1: EPIC spectra (*upper panel*) and residuals in units of data/model ratio (*lower panel*), for the spectral fit in Tab. 2; MOS1: *black*; MOS 2: *red*; pn *green*. Each data point corresponds to a signal-to-noise ratio ≥25.

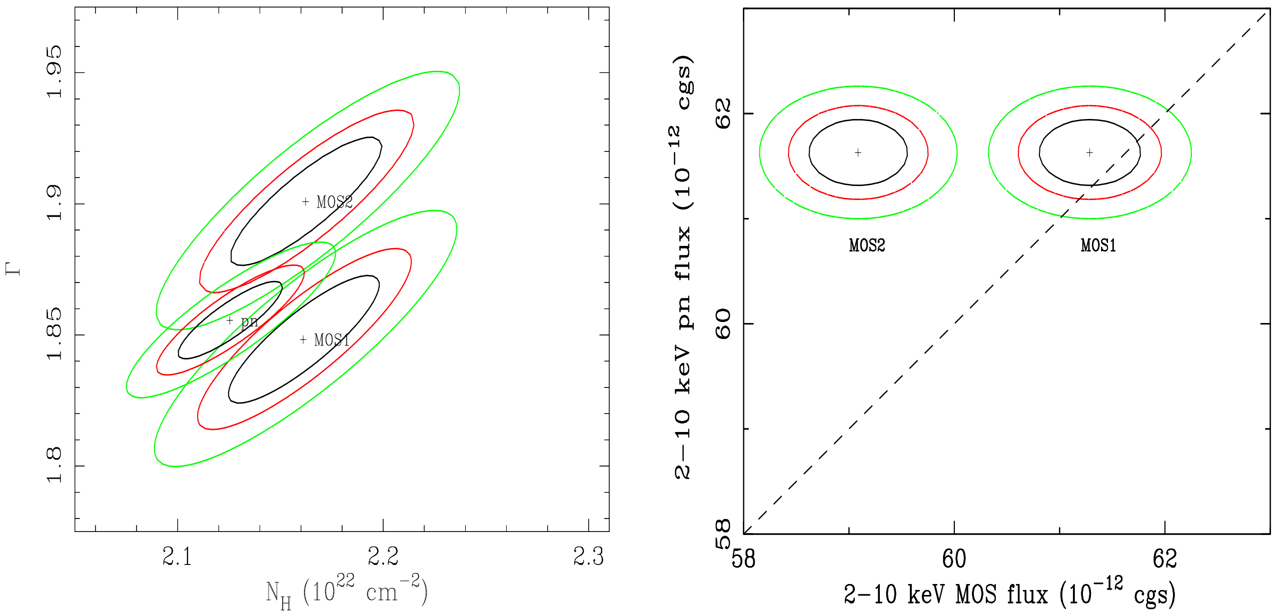

Figure 2: *Left panel*: iso-χ^2 contour plots for N_H versus Γ. Contours are at 68%, 90%, and 99% confidence levels for two interesting parameters. *Right panel*: iso-χ^2 contour plots for the MOS 2–10 keV observed flux versus the pn flux in the same energy band. The *dashed line* indicates the locus of equal fluxes

are basically consistent within the statistical uncertainties. The difference between the results in the MOS2 and in the other cameras may be related to a $\simeq 1'$ shift between the nominal boresight position and the optical axis, which is still not perfectly accounted for by the response matrices averaging.

2.1.2 PKS0558-504, Obs.#0125110101, Rev.#84

Here we analyze the first exposure of the Rev.#84 observation of PKS0558-504 made with the pn detector in Full Frame mode and the two MOS cameras in Large Window mode. All of the cameras use the medium filter and suffer from a modest amount of pile-up (the count-rate is 14.0 s^{-1} for pn, and 6.2 s^{-1} for the MOS cameras).
Spectra were initially extracted from circular regions centered on the source using `especget` and were tested for pile-up using `epatplot`. All of the plots show significant deviation from the expected pattern fraction curves (Fig. 3) and it was necessary to exclude the inner $5''$ and $10''$

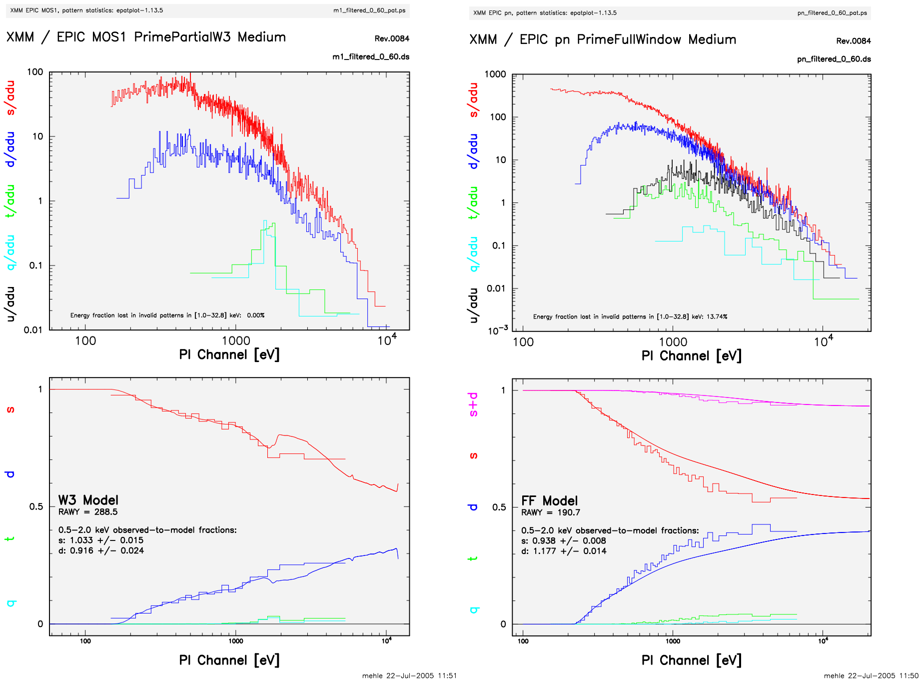

Figure 3: The `epatplot` output for circular extraction regions about PKS0558-504 for MOS-1 (`left`) and pn (`right`) in Rev.#84 (*i.e.*, before excising of the PSF core)

from the MOS and pn extraction regions, respectively to get good agreement with the model[1]. The pn data were screened for high flaring background, resulting in an exposure time of 4.7 ks. These time intervals were used to extract events for all the three cameras to ensure that source variability would not affect the comparison of the camera spectra. Spectra were extracted from annuli of 5–60 (MOS) and 10–60 (pn) arc-seconds about the source with the pn time windows and standard selections of (`FLAG==0 && PATTERN<=4`) (pn) and (`#XMMEA_EM && PATTERN<=12`) (MOS) applied. Background spectra were extracted from source-free areas of sky near to the

[1] Users may refer to XMM-NEWS#31 (`http://xmm.vilspa.esa.es/external/xmm_news/news_list/xmm_news-2003-03-27.shtml`) for a discussion on this analysis approach

Table 3: Rev.#84 PKS0558-504 best-fit parameters for a power-law plus two black-body model with the hotter black-body having a fixed temperature of 150 eV. kT and N_{BB} are the temperature and normalization of the black-body components. F is the measured flux.

Instrument	Γ	kT^1_{BB} (eV)	N^1_{BB} 10^{-5}	kT^2_{BB} (eV)	N^2_{BB} 10^{-6}	F (0.2–2 keV) (10^{-11} erg cm^{-2} s^{-1})	F (2–10 keV)	χ^2/dof
pn	$2.26\pm^{0.08}_{0.07}$	67 ± 4	29 ± 4	150	$96\pm^{16}_{19}$	2.15	0.80	109/129
MOS1	$2.16\pm^{0.10}_{0.09}$	$62\pm^{5}_{4}$	$40\pm^{8}_{7}$	150	$93\pm^{20}_{23}$	2.15	0.89	121/118
MOS2	$2.18\pm^{0.10}_{0.09}$	58 ± 4	$45\pm^{11}_{7}$	150	96 ± 21	2.20	0.90	132/117

target and response matrices were created using `arfgen` and `rmfgen` in the standard manner. The source spectra were grouped to give a minimum number of 25 counts per channel and a factor of three by which to oversample the EPIC energy resolution and were fit independently with a model constituted by a power-law and two black-bodies attenuated by absorption in cold gas fixed at the measured galactic value of 4.4×10^{20}cm^{-2} (O'Brien et al. 2001). The hotter black-body temperature was poorly constrained and so was fixed at 150 eV in the fits. The best-fit parameters are given in Table 3. The fits for the three EPIC cameras are seen to be in good agreement and the fluxes are very similar: at low energies derived fluxes agree within within the errors. In the 2–10 keV band, the measured pn flux was found to be $\sim$ 10% lower than the MOS flux.
The best fits and residuals are presented for the three cameras in Fig. 4.

2.1.3 PKS0558-504, Obs.#0129360201, Rev.#153

Here we analyze the EPIC observations obtained in Rev.#153: a pn exposure was performed in Small Window mode and MOS1 and MOS2 in Large Window mode with the Thin1 filter in place for all these exposures. The ODF was processed with the `epproc` and `emproc` tasks to generate MOS and pn calibrated event lists.
The exposures were free of flaring background and the total 10.7 ks (pn) and 7.9 ks (MOS) could be taken into account.
According to the `epatplot` created pattern statistics (Fig. 5), the EPIC window mode observations are not significantly affected by pile-up. This holds especially true for the pn Small Window exposure whereas there might be some marginal deviations of the MOS data from the model. The pn Full Frame mode exposures also taken in Rev.#153 are strongly affected by pile-up, and therefore were excluded from this report.
Checking the light curves of PKS0558-504 obtained during the EPIC partial window observations (Fig. 6), the source was found to be variable. The further analysis of the spectra obtained with the three different EPIC cameras therefore was restricted to the time interval in which all instruments were simultaneously collecting data. This reduced the effective exposure time to 7.0 ks. We used `xmmselect` to display the EPIC data in sky coordinates and to define source and background regions for `especget`: Source spectra have been extracted from circular areas centered on PKS0558-504 and background spectra from source-free rectangular regions from the same CCD. Standard quality flag and pattern selections, as defined in `especget`, have been adopted: `((FLAG==0) && (PATTERN<=4))` (pn) and `(#XMMEA_EM && (PATTERN<=12))` (MOS). Response matrices have been generated on the fly by `especget` calling `rmfgen` and `arfgen`, with

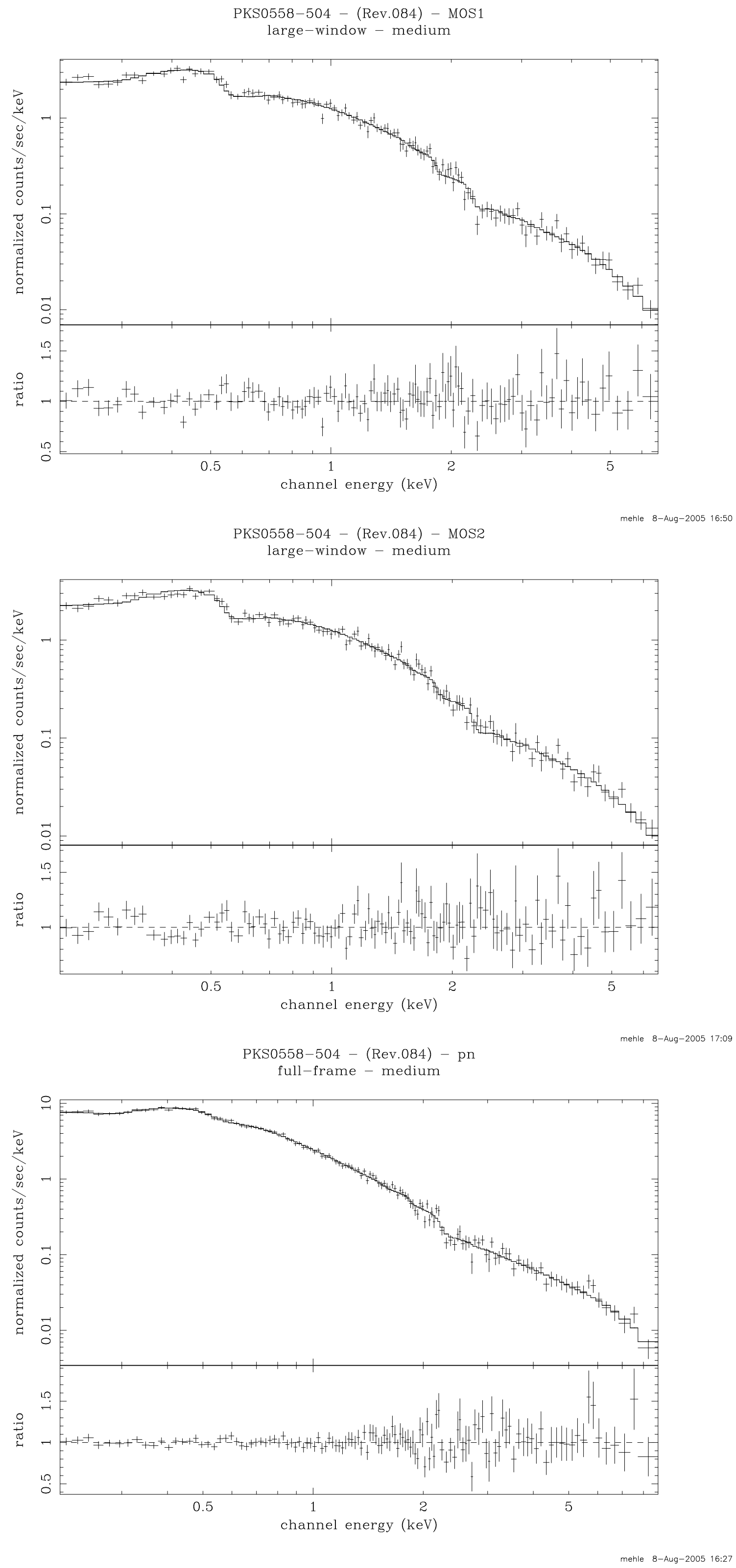

Figure 4: Spectra and residuals for MOS1 (*upper*), MOS2 (*middle*) and pn (*lower*) fits to the Rev.#84 observation of PKS0558-504 (after excision of the PSF core)

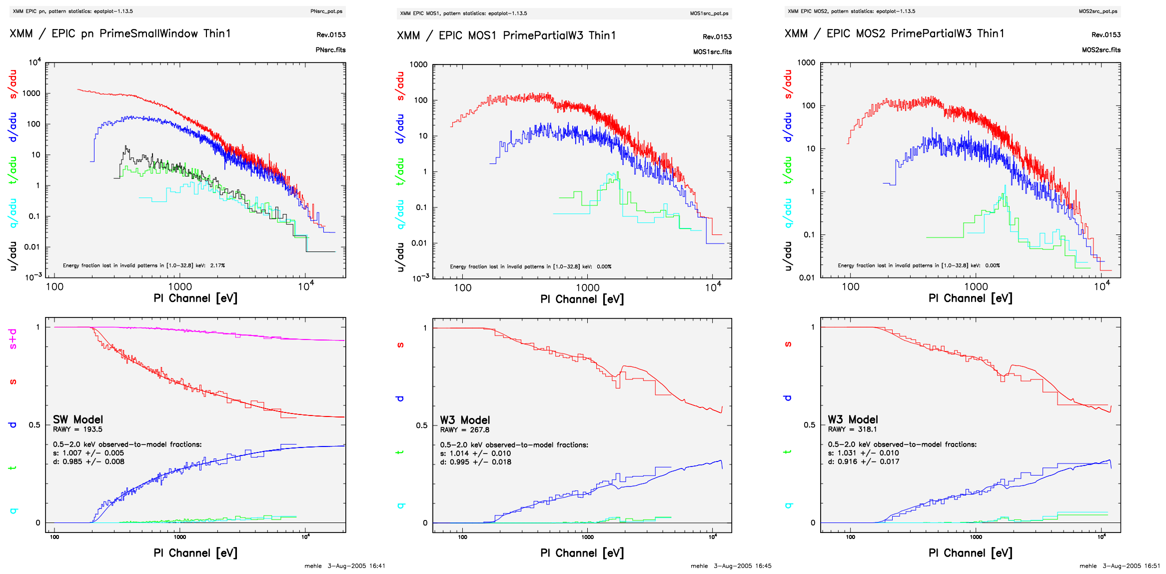

Figure 5: PKS0558-504 pattern statistics of the pn Small Window (*left panel*), and the MOS1 and MOS2 Large Window (*middle & right panel*) exposures in Rev.#153, produced by the SAS task `epatplot`.

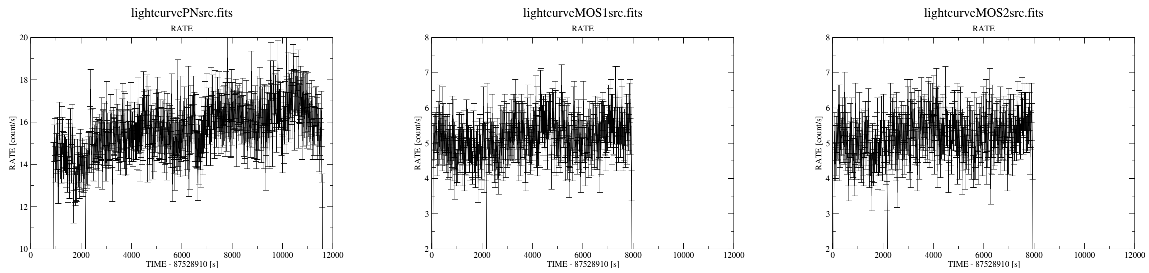

Figure 6: PKS0558-504 light curves of the pn Small Window (*right panel*), and the MOS1 and MOS2 Large Window (*center & left panel*) exposures in Rev.#153. The bin-size is 20 s and the energy selection 0.15-10 keV.

Table 4: PKS0558-504 best-fit parameters for pn Small Window mode and MOS Large Window mode observations in Rev.#153. N are the normalizations and kT the temperatures of the blackbody components. F is the measured model flux.

	Γ	N_Γ (10^{-4})	kT^1_{BB} (eV)	N^1_{BB} (10^{-5})	kT^2_{BB} (eV)	N^2_{BB} (10^{-6})	F(0.2-2 keV) (10^{-11} erg cm^{-2} s^{-1})	F(2-10 keV)	χ^2/ dof
pn	2.18 ± 0.04	$59\pm^2_3$	53 ± 3	37 ± 5	$142\pm^7_6$	139 ± 10	2.53	1.17	183/197
MOS1	2.19 ± 0.07	61 ± 4	$56\pm^3_6$	$35\pm^8_{10}$	$146\pm^{14}_{15}$	$94\pm^{16}_{17}$	2.41	1.17	152/165
MOS2	$2.25\pm^{0.07}_{0.06}$	67 ± 4	$58\pm^6_{12}$	$23\pm^{38}_6$	$128\pm^{19}_{16}$	$97\pm^{41}_{15}$	2.43	1.20	137/166

Table 5: PKS0558-504 best-fit parameters of simultaneous pn, MOS1 and MOS2 data fitting. N are the normalizations and kT the temperatures of the blackbody components. C marks the fit constants for pn/MOS1/MOS2, respectively, and F the model flux for pn.

Γ	N_Γ (10^{-4})	kT^1_{BB} (eV)	N^1_{BB} (10^{-5})	kT^2_{BB} (eV)	N^2_{BB} (10^{-6})	C (%)	F(0.2-2 keV) (pn, 10^{-11} erg cm^{-2} s^{-1})	F(2-10 keV)	χ^2/ dof
$2.20\pm^{0.04}_{0.03}$	$62\pm^{23}_{18}$	55 ± 2	$34\pm^5_3$	$141\pm^5_8$	$120\pm^{11}_7$	100/95/97	2.52	1.20	540/526

`detmaptype=psf`.
Source spectra have finally been grouped with a minimum number of 25 counts per channel and a factor of three by which to oversample the EPIC energy resolution.
The pn, MOS1 and MOS2 spectra have been fit individually with a model constituted of a power-law and two blackbody components all affected by foreground absorption fixed at the Galactic value of 4.4×10^{20} cm^{-2} (*baseline model*; the third blackbody envisaged by O'Brien et al. (2001) is actually not required by the fit of this dataset).
The power-law component dominates above 2 keV, the blackbodies account for the bulk of the prominent soft X-ray excess. The spectra and best-fit models are shown in Fig. 7, together with the data/model ratio residuals. Best-fit parameters and results are summarized in Tab. 4. The fits for the individual EPIC cameras (pn, MOS1 and MOS2) agree well (cf. Table 4). We note that the fit parameters to the MOS2 spectrum show somewhat larger errors than the ones for the pn and MOS1.
We found flux differences between pn and MOS of the order of 5% in the soft energy range 0.2 - 2 keV (where systematic fit residuals are found - cf. Fig. 8), whereas fluxes agree to better than 3% in the energy band 2 - 10 keV.
In addition to the camera specific fits, a simultaneous fit of pn, MOS1 and MOS2 Rev.#153 data using the baseline model was performed between 0.2 and 10 keV (see the left panel of Fig. 8). A constant factor was introduced to account for absolute flux discrepancies between the individual EPIC cameras: the factor was fixed to 100% for pn and let a free parameter for the two MOS. The residuals (cf. the right panel of Fig. 8) show that a general good agreement between the cameras is achieved: the discrepancy in the cross calibration of the EPIC instruments for this source, modes and filter are less than 10% in the ratio data/model. The discrepancies are somewhat larger around the 1.8 keV Si-edge. For completion the best fit parameters obtained are given in Tab. 5.

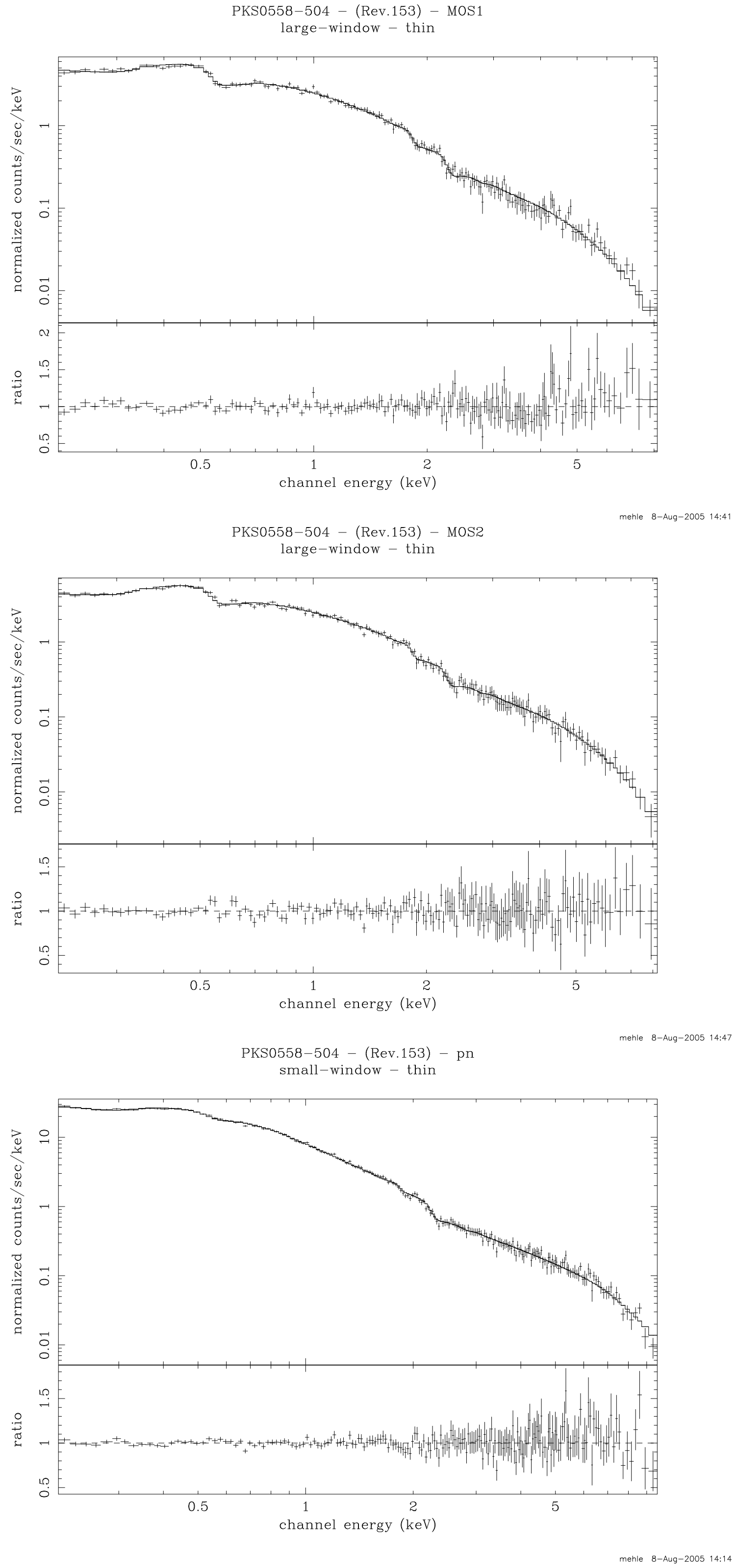

Figure 7: PKS0558-504 MOS1 (*top*), MOS2 (*top center*) and pn (*bottom*) spectra (*upper panel*) and residuals in units of data/model ratio (*lower panel*) when the baseline model is applied to the spectrum of the Large Window exposure in Rev.#.153.

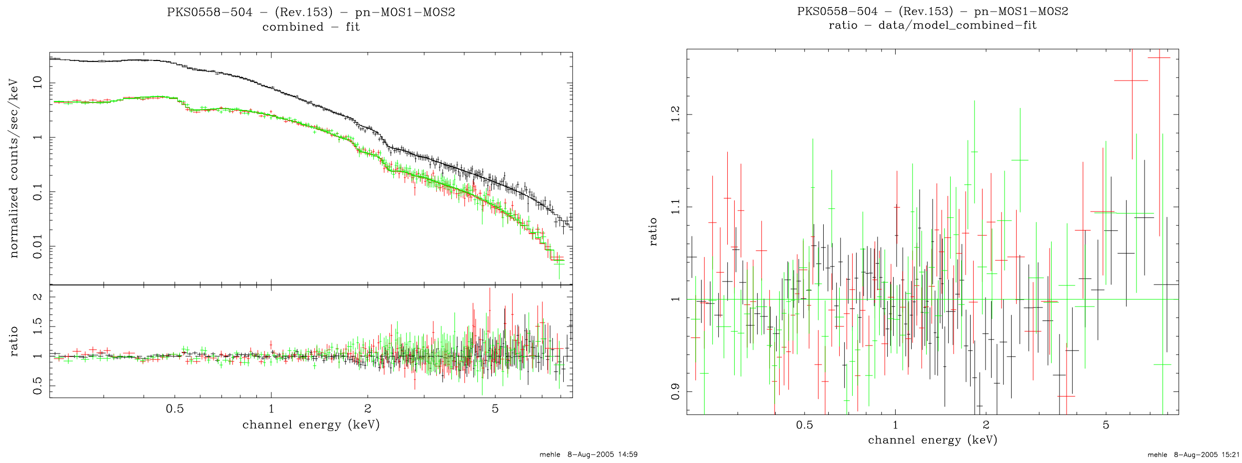

Figure 8: *Left panel*: PKS0558-504 pn (black), MOS1 (red) and MOS2 (green) spectra together with residuals in units of data/model ratio (*lower panel*) when the baseline model with additional factors for the three cameras is simultaneously applied to the spectra of the Small Window (pn) and Large Window (MOS) exposures of Rev.#153. *Right panel*: PKS0558-504 pn (black), MOS1 (red) and MOS2 (green) combined fit residuals in units of data/model ratio. Data were re-binned for clarity and plotting purposes.

Table 6: MOS/pn normalization constants for the fit of the Rev.#1012 observation of H1426+428. Statistical errors are ≃0.05.

	SASv6.1	SAS v6.5
MOS2 (`FLAG==0`)	0.98	1.02
MOS1 (`FLAG==0`)	0.89	0.98
MOS2 (`#XMMEA_EM`)	1.00	1.02
MOS1 (`#XMMEA_EM`)	0.96	0.99

2.2 MOS low sensitivity patch

In this Section, the pn/MOS flux consistency on a recent observation is verified, after the discovery of a low sensitivity patch close to the MOS boresight and a hot column in MOS1 CCD1. The tests have been performed on an observation of the blazar H1426+428 performed in Rev.#1012. During this observation a hot column was detected in the central MOS1 CCD, 9 pixels away from PSF center.
Spectra were Extracted for PN (`FLAG==0`), MOS2/1 (`FLAG==0` and `#XMMEA_EM`) for SAS 6.1 and SAS6.5. Using `FLAG==0`, three columns, the hot column plus adjacent columns, are ignored. Using `#XMMEA_EM`, only the hot column is ignored. The used fit model was a simple photoelectrically absorbed (Wilms' et al. (2000) abundances) power-law. The absorber column density was fixed to $N_H = 1.36 \times 10^{20}$ cm^{-2}. This model describes the data sufficiently well, to allow us to investigate the differences in flux and spectral shape between the spectra of the two SAS versions. Combined fits were performed, including normalization constants with PN fixed to 1.0. The results are summarized in Tab. 6. `arfgen` takes now properly into account the flux lost due the ignored columns. Using SAS6.1, MOS1 disagreed up to 11% for `FLAG==0` (3 columns were

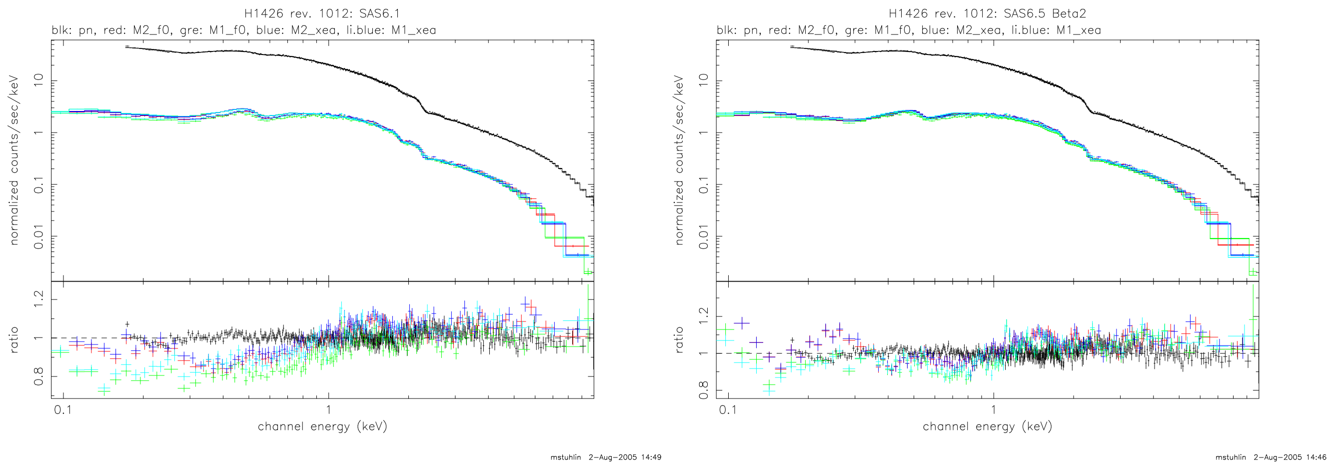

Figure 9: Comparison of the quality of spectral fitting among the EPIC camera when the H1426+428 data are reduced with SASv6.1 (*left panel*) and SASv6.5 (*right panel*)

Table 7: MOS/pn normalization constants for the fit of the observation of RXJ1856 (Obs.#0165971901), with respect to the MOS2 spectrum extracted with **#XMMEA_EM**

MOS2 (`FLAG==0`)	$1.022\pm^{0.014}_{0.008}$
MOS1 (`#XMMEA_EM`)	$0.651\pm^{0.012}_{0.006}$
MOS1 (`FLAG==0`)	$0.765\pm^{0.015}_{0.006}$

ignored). Using SAS6.5, MOS and PN agree within ±2% independent of the employed flags. (see Fig. 9). Differences are within about ±10% across the whole sensitive bandpass.
However, users are recommended to exercise caution when analyzing and interpreting data, when hot columns are located 1 or 2 pixels away from the PSF center. This occurs, for instance, in a recent observation of RXJ 1856 (Obs.#0165971901). The adjacent columns to the hot one show a strong decrease of counts, but are not flagged as bad by `embadpixfind`. Using SAS6.1, these columns were flagged as bad. This leads to the extraction of a wrong MOS spectrum even if `#XMMEA_EM` is used, as adjacent columns are taken into account, and the PSF center is not clearly defined. In this case, it is advisable to use `FLAG==0` for the extraction of the spectra, which leads to ignoring adjacent columns. Still the results are not satisfactory (Tab. 7). This is probably due to the still incorrect determination of the PSF centroid.

3 EPIC-pn fast modes

3.1 Her-X1–Validation of EPIC-pn Timing mode

XMM-Newton observed Her-X1 ($\alpha_{2000} = 16^h57^m49^s.80$, $\delta_{2000} = +35°20'32''.6$) , several times. The observation used in this report took place on January 26, 2001, revolution 207, lasting more than 9000 seconds.
For this analysis only EPIC-pn data have been used. We used the following setting to extract source and background regions, respectively: `((RAWX,RAWY) IN box(36.5,100,25,99.5,0))`,

`((RAWX,RAWY) IN box(5,100.75,4.5,99.25,0))` Spectra have than been extracted using single and double events neglecting the events at CCD borders and events lower than 0.5 keV where data should not be used due to the high noise below 0.5 keV in EPIC-pn Timing Mode.
All response files have been created using SAS 6.5. The spectra have been fit with a model constituted by photoelectric absorption (the `wabs` implementation in XSPEC was used), a power-law, a disk blackbody, and four Gaussian lines (two of them intrinsically broad). Several residual features are known to be due to current uncertainties in the calibration. Fig. 10 shows a plot of Her-X1 (data and model) of the best fit to the EPIC-pn Timing mode spectrum. The best-fit

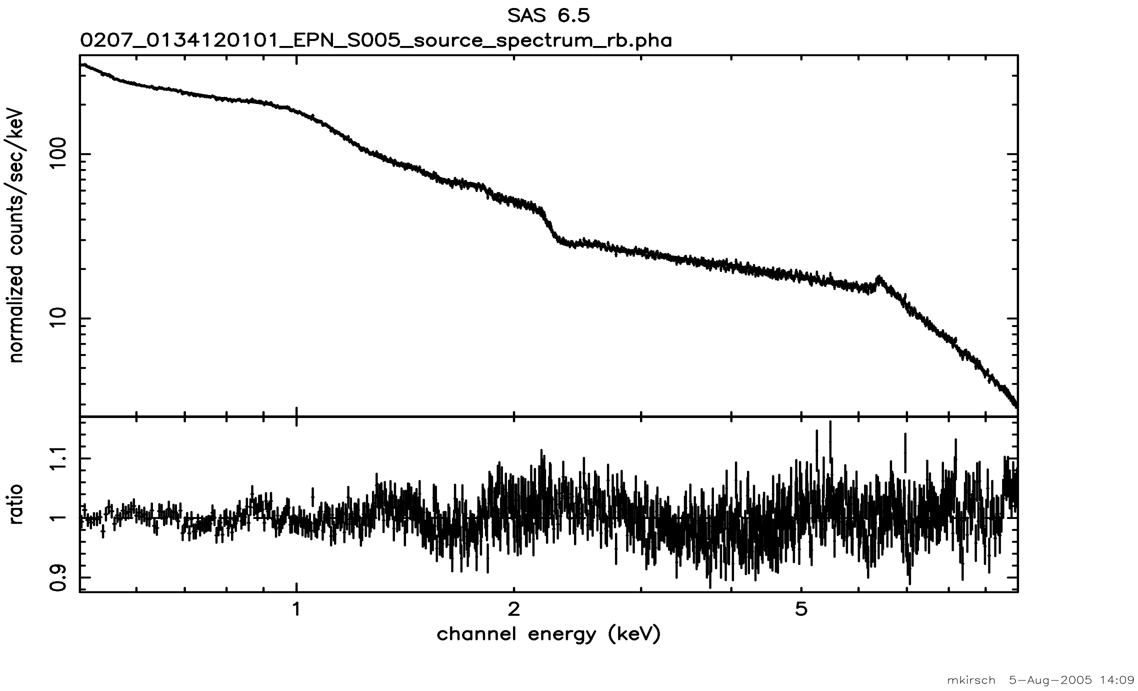

Figure 10: Spectrum of Her-X1 in EPIC pn Timing mode

parameters and results are summarized in Tab. 8.

Table 8: Her-X1 best-fit parameters. The 0.5 keV Gaussian and the sigma of one iron line have been frozen. E_i^C indicates the centroid energy of the i-th line, σ_i its intrinsic width

χ^2/ dof	Γ	Tin [eV]	N_{BB} [10^4]	E_1^C [keV]	σ_1 [keV]	E_2^C [keV]	σ_2 [keV]
1215.0/848	$0.861 \pm^{0.006}_{0.004}$	$177 \pm^{5}_{7}$	$1.52 \pm^{0.4}_{0.2}$	$0.5^\dagger$	$0.005^\dagger$	$0.9626 \pm^{0.032}_{0.037}$	$0.143 \pm^{0.004}_{0.002}$
				E_3^C [keV]	σ_3 [keV]	E_4^C [keV]	σ_4 [keV]
				$6.564 \pm^{0.029}_{0.027}$	$0.436 \pm^{0.052}_{0.045}$	$6.435 \pm^{0.011}_{0.016}$	$0.005^\dagger$

†frozen

3.2 Crab – Validation of EPIC-pn Burst mode

XMM-Newton observed the Crab Nebula ($\alpha_{2000} = 05^h34^m31^s.97$, $\delta_{2000} = +22°00'52''.1$) - encompassing the most famous pulsar of X-ray astronomy (Kirsch et al. 2005) - in Rev.#234,

411, 698, 700, 874 and 955 using the EPIC-pn-fast modes (*i.e.* Timing and Burst Modes). For spectral analysis only Burst mode data of the Crab are useful, since the spectra will be piled-up in Timing mode. However the Timing mode observations can be used for timing analysis. We used the following setting to extract source and background regions: `((RAWX,RAWY) IN box(35.,71.5,20,70,0))`, and `((RAWX,RAWY) IN box(6,64,5,63.5,0))`, respectively. Spectra in the energy range 0.3–10 keV have than been extracted for Burst mode observations using single and double events only neglecting the events at CCD borders.
The spectra have been fit with a model constituted by photoelectric absorption (`wabs` implementation in XSPEC), and a power-law setting abundances to Wilms et al. (2000) and cross-sections as in Verner et al. (1997). Several residual features are known to be due to current uncertainties in the calibration. Fig. 11 shows the Crab (data and model) of the best fit to the EPIC-pn Burst mode spectrum. The best-fit parameters and results are summarized in Tab. 9. Note that

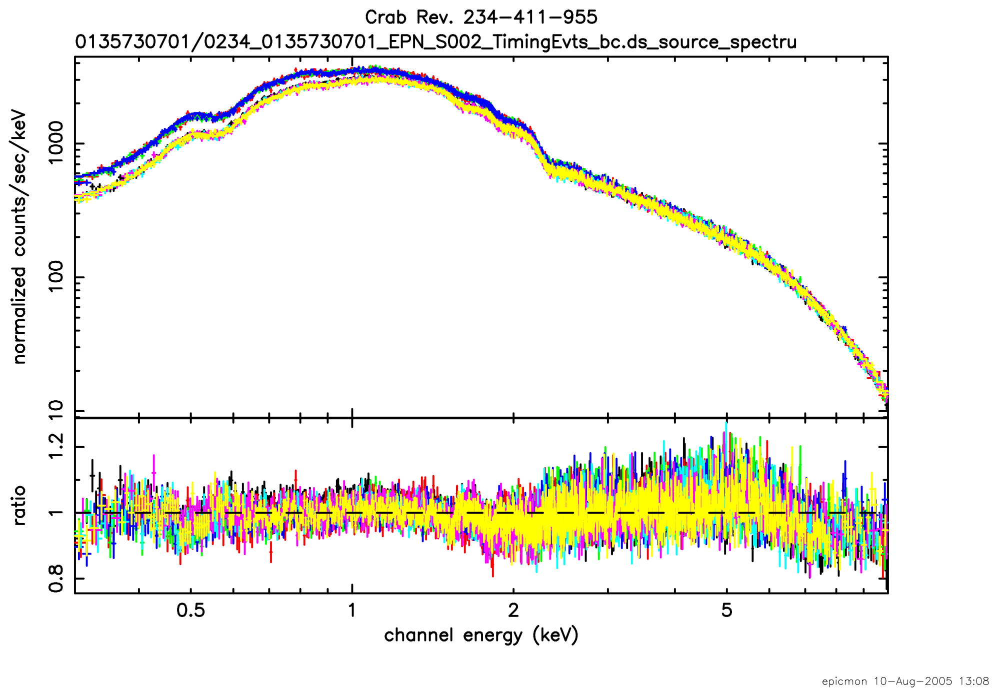

Figure 11: Spectra of the Crab in EPIC Burst mode

Table 9: Crab best fit parameters.

Instrument	Γ	$Norm$ [photons $(keV)^{-1}$ cm^{-2} s^{-1}] @ 1 keV	N_H [10^{21}]	χ^2/ dof [keV]
p-n	$2.057\pm^{0.002}_{0.002}$	$7.13\pm^{0.01}_{0.01}$	$3.848\pm^{0.001}_{0.001}$	13635/10138

the normalization of the Crab from that observations is not correct since the Crab is not fully imaged in the CCD. However extraction regions are now correctly treated by `arfgen` in Burst mode since SAS 6.1. This means that the normalization in Tab. 9 properly represent the flux of the section of the Crab Nebula, which falls onto the pn Burst Mode field-of-view.

3.3 Relative timing of EPIC-pn

The EPIC-pn event analyzer (EPEA) uses the CDMU 1 Hz clock pulse to increment an internal 15 bit wide counter (FTCOARSE) and to reset a 16 bit sub-second (FTFINE) counter which is clocked with 48828.125 Hz. Thus the EPIC-pn CCD data frames are time stamped with a resolution of 20.48 ms by FTCOARSE/FTFINE pairs. In an ODF they form two columns in the first table of the EPIC-pn Auxiliary Data File (AUX) which are accessed by SAS in the process of converting frame counters to absolute photon arrival times.

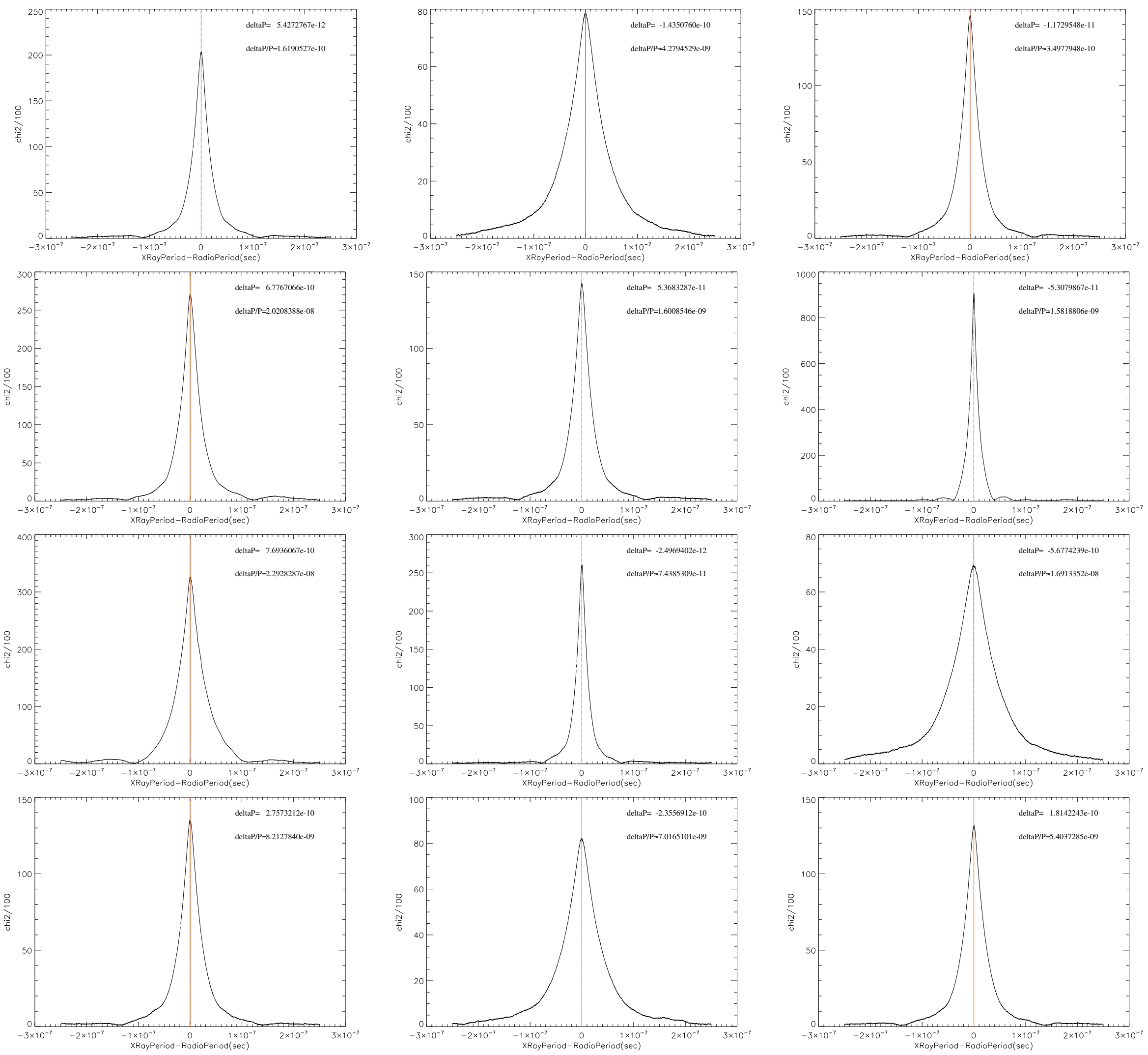

Figure 12: χ^2 epoch folding for different Crab observations. Note that all possible time jumps are corrected in the fast EPIC-pn modes and the χ^2 distributions is smooth as it should be.

In mid-2000 it was first discovered that the EPIC-pn AUX data exhibit certain kinds of anomalies whose frequency of occurrence is variable and apparently unrelated to camera mode, observing time or duration. This remains valid until today, i.e. some data sets are completely free of any problems others are heavily affected. Obviously all these problems need to be corrected for, as otherwise the event times turn out wrong. This is especially critical, as a single shift in FT-COARSE time will cause all subsequent times to be wrongly shifted by the same amount. Pulse

profile analyzes with a data set that contains a single or multiple undetected and uncorrected such time jump will then be inconclusive because all photons after the instant of the time jump will be out-of-phase. This can result in a pulse peak broadening, phase shift or the appearance of spurious pulse components. Absolute timing analysis was likely impossible for obvious reasons. In the past these anomalies have all been seen and led to difficulties in the interpretation of obtained tentative results.
The SAS since the early days can reliably detect and correct for the anomalies. However, the detection logic seems to fail in some cases, with the consequences described above.
As of the SASv6.0 release we were in a state that all problems are reliably found and corrected for the fast EPIC-pn modes (Timing and Burst) however there might be still some rare cases of time jumps. This is still under investigation with a bulk reprocessing of all XMM-Newton data.
Fig. 12 shows χ^2-epoch folding for different Crab observations, with a resolution of $\simeq 1 \times 10^{-10}$ s.
We performed χ^2-distributions of epoch folding for all Crab observations in the fast EPIC-pn modes. Each observation was folded using the radio period as a start value and the epoch of the respective radio period. We determined the X-ray period by calculating the weighted mean of the periods in each epoch folding using all periods for χ^2 values greater than 65 % of the maximum χ^2. We give the characteristic value for relative accuracy of timing analysis $\Delta P/P$ where $\Delta P = P_{radio} - P_{xray}$ and $P = P_{radio}$.
Fig. 13 shows the result of that analysis. The relative timing of XMM-Newton is considered better than some 10^{-8}.

4 XMM-Newton instrument cross-calibration

The observation of the radio-loud Narrow-line Seyfert 1 galaxy PKS0558-504 ($\alpha_{2000} = 05^h59^m47^s.00$, $\delta_{2000} = -50°26'51''.0$) from Rev.#153 was used to access the status of cross calibration for all x-ray instruments on board XMM. We used the following exposures for the different instruments: EPIC-pn: S004, EPIC-MOS1: S004, EPIC-MOS2: S006, RGS1: S010, RGS2:S011. Since the source was found to be variable during the observation we restricted the analysis to the time interval in which all instruments operated simultaneously between 2000-10-10T01:48:53 and 2000-10-10T03:46:38. Based on recent literature, the SIMBAD coordinates of this object have been revised by more than $12''$ but we ignored this change in specifying the RGS source coordinates and used the observation pointing values given above which correspond closely with the detected EPIC position.
We used the following setting to extract source and background regions. pn source spectra were extracted from a circular region of $37''$ radius; its background spectra were extracted from a similar region, at the same height in detector coordinates. MOS source spectra were extracted from a somewhat larger region ($108''$), after excising the innermost $9''$ to reduce pile-up; their background was extracted from an offset large ($\simeq 230''$) offset circular region on the same CCD as the source. Spectra were extracted using single and double events, neglecting events at CCD borders and events lower than 0.15 keV. The spectra were modeled by a photoelectrically-absorbed combination of power-law and blackbody, setting abundances to Wilms et al. (2000), and allowing overall free normalization among the instruments. Fig. 14 shows a plot of PKS0558-504 (data and model) of the best fit to all spectra. The best-fit parameters and results are summarized in Tab. 10.

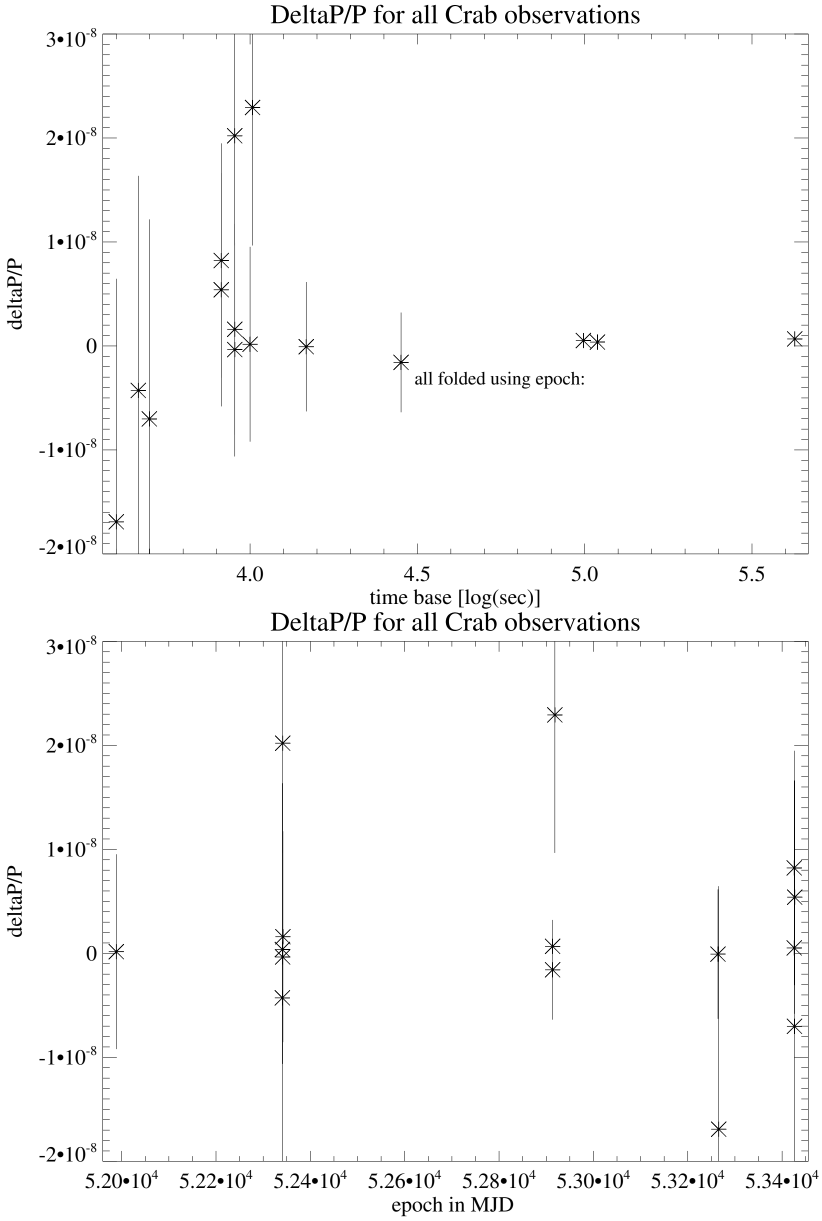

Figure 13: ΔP/P for all XMM-Newton Crab observations (EPIC-pn). *Upper panel*: the x-axis gives logarithmically the total time base of the observation (for longer observations the relative timing accuracy is obviously better.). *Lower panel*: the x-axis gives the epoch in MJD.

5 Conclusions

The main conclusion of the EPIC SASv6.5 SV exercise can be summarized as follows:

- SASv6.5 can reduce data taken with all the EPIC scientific modes
- event list produced with the `chains` and the `procs`, albeit not identical, yield scientifically indistinguishable results

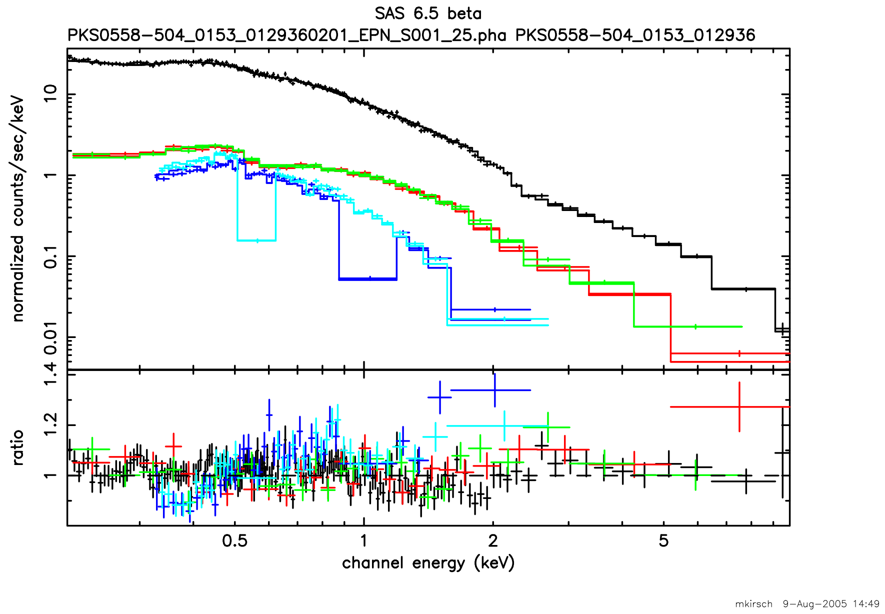

Figure 14: Spectra of PKS0558-504 with all EPIC X-ray instruments

Table 10: PKS0558-504 best-fit parameters. C indicated the normalization constant among the X-ray instruments

Instrument	Γ	1 keV N_Γ [10^{-3} cgs]	N_H [$10^{20} cm^{-2}$]	kT_{BB} [eV]	N_{BB} [10^5]	C	χ^2/ dof
EPIC-pn	$2.71\pm^{0.02}_{0.02}$	$7.66\pm^{0.06}_{0.06}$	4.43 ± 0.02	$1.48\pm^{0.17}_{0.14}$	$6.01\pm^{0.8}_{0.44}$	1	2344/2102
EPIC-MOS1	†	†	†	†	†	0.99 ±0.02	-
EPIC-MOS2	†	†	†	†	†	1.03 ±0.02	-
RGS1	†	†	†	†	†	0.90 ±0.02	-
RGS2	†	†	†	†	†	0.90 ±0.02	-

†linked to pn

- the quality of spectral fitting is significantly improved with SAS v6.5. Residuals are within ±5% for all Imaging and Timing Modes across the whole sensitive bandpass
- the relative timing accuracy of the pn camera is $\lesssim 3 \times 10^{-8}$
- the flux cross-calibration among the EPIC cameras is better then 5%, once again improving with respect to previous SAS SV excercises
- SASv6.5 corrects well for the low sensitivity patch recently discovered close to the MOS camera boresight, as well as for any associated MOS1 bright columns, *as long as* the latter features are not too close (1–2 pixels) to the centroid of the PSF
- the cross-calibration among the X-ray instruments on board XMM-Newton improves significantly with SASv6.5. Nonetheless, cross-calibration is a continuous efforts, whose development is mainly asynchronous with the SAS releases. Users are recommended to refer to the EPIC Calibration Status Document

Table 11: XMM-Newton instrument scientific modes supported by the SAS and the PPS

Mode	Processed by SAS?	Processed by PPS?
	MOS	
Full Frame	Y	Y
Large Window	Y	Y
Small Window	Y	Y
Timing Uncompressed	Y	Y
	pn	
Full Frame	Y	Y
Large Window	Y	Y
Small Window	Y	Y
Fast Timing	Y	Y
Fast Burst	Y	Y
Extended Full Frame	Y	Y
	RGS	
Spectroscopy	Y	Y
	OM	
Image Mode	Y	Y[a]
Fast Mode	Y	Y[a]
Full Frame Low Resolution	Y	Y[a]
Full Frame High Resolution	Y	Y[a]
Science User Defined	Y	Y[a]

[a]except for exposures taken in optical and UV grism

(`http://xmm.vilspa.esa.es/docs/documents/CAL-TN-0018-2-4.pdf`) for the most recent updates on this topic

References

Kirsch M.G.F., et al., 2005, SPIE, in press (astro-ph/0508235)
O'Brien P.T., et al., 2001, A&A, 365, L122
Verner D.A., et al., 1996, ApJ, 465, 487
Warwick R.S., et al., 2001, A&A, 365, 248
Wilms J., et al., 2001, ApJ, 542, 914

Appendix A: Matrix of supported instrument modes by SAS v6.0

In Tab. 11 we show the list of science instrument modes which can be processed by the SAS, and are currently being routinely processed by the pipeline.

Appendix B: *Can*s and *Can't*s for SAS v6.0

This page provides a quick summary of what can and what can't be done with the SAS version discussed in this document. Moreover, it summarizes the status of the PPS data product processing.

- What SAS can do now (in brackets the SAS module responsible for the task)
  - run tasks either from the command line or through the interactive GUI
  - create script and session logs
  - create Calibration Index Files tailored to the user analysis conditions (`cifbuild`)
  - apply barycentric corrections (barycen)
  - With EPIC data
    * generate calibrated event lists (`e[mp]proc`, `e[mp]chain`)
    * extract scientific products (light curves, spectra, images) for all instrumental modes (`evselect`, `xmmselect`) from event lists. Event lists can be filtered by the user (`selectlib`).
    * run source detection algorithms on images (`edetect_chain`)
    * create Good Time Intervals from time-varying data (`tabgtigen`) and apply them to the scientific product extraction
    * create response matrices (*arfgen*; `rmfgen`) for all modes, both for point-like and extended sources
  - With RGS data
    * generate calibrated event lists (`rgsproc`)
    * run the reduction meta-task (`rgsproc`) from different entry points and to different end levels
    * extract source and background 1st and 2nd order spectra (`rgsspectrum`; run automatically through `rgsproc`)
    * create customized source lists or modifying existing EPIC source lists (`rgssources`) for scientific product extraction
    * produce plots of the dispersion versus cross-dispersion and energy versus dispersion planes, to verify the quality of the foreground and background extraction regions (`rgsimplot`).
    * generate a response matrix for a given source spectrum (`rgsrmfgen`)
    * create first- and second-order fluxed spectra (`rgsfluxer`)
  - with OM data
    * produce flat-fielded geometrically-corrected sky images for all lenticular filters, both for individual windows and for all windows combined, using image mode data
    * produce for individual windows and all windows combined, source lists, including color information for all lenticular filters using fast and image mode data
    * produce light curves time-series using fast mode data
    * produce tracking history information
    * extract wavelength and flux-calibrated OM grism spectra (`omgchain`, `omgsource`)
- What SAS cannot do yet

- create RGS exposure-corrected light curves
- automatically create RGS spectra (and the corresponding response matrices) for extended sources

- Which PPS Data Products are available
  - EPIC
    * Exposure and observation images and image plots
    * Exposure maps and sensitivity images
    * Exposure and observation source lists
    * Calibrated and flagged event lists
    * Flare background time-series
    * HTML summaries
  - OM
    * Science window detector sky images and image plots
    * Observation source lists
    * Tracking star time series and history plots
    * Mosaiced filter-specific images and image plots
    * Fast Mode source time-series
    * HTML summaries
  - RGS
    * Spatial and energy-wavelength images and plots
    * Exposure maps
    * Calibrated and flagged event lists
    * Source lists
    * First- and second-order source and background spectra and spectral plots
    * Flare background time-series
    * First-order response matrices
    * HTML summaries
  - General
    * HTML ODF and PPS summaries
    * PPS script log, product indices
    * Calibration index files and attitude time series

Users are reminded that exposures with not scientific filters (*e.g.*: EPIC CAL_CLOSED, OM BLOCKED) are not intended to be processed by the PPS. OM grism data are currently not processed by the PPS.